ChemComm

Exciton coupling chirality in helicene-porphyrin conjugates

Journal:	*ChemComm*
Manuscript ID	CC-COM-06-2021-003314.R1
Article Type:	Communication

COMMUNICATION

Exciton coupling chirality in helicene-porphyrin conjugates

Received 00th January 20xx,
Accepted 00th January 20xx

Kais Dhbaibi,[a] Paola Matozzo,[a] Laura Abella,[b] Marion Jean,[c] Nicolas Vanthuyne,[c] Jochen Autschbach,[*b] Ludovic Favereau,[*a] and Jeanne Crassous[*a]

DOI: 10.1039/x0xx00000x

Enantiopure helicene-porphyrin conjugates were prepared. They show strong changes in their circular dichroic response as compared to classical helicene derivatives, with highly intense bisignate Exciton Coupling (EC) signal and $\Delta\varepsilon$ values up to 680 M^{-1} cm^{-1} for the Soret band. They also display circularly polarized fluorescence in the (far-)red region, with dissymmetry factors up to 7.10^{-4}.

Helicenes are helical π-conjugated molecules with ortho-fused aromatic rings.[1] Their strong chiroptical properties are appealing in several fields of research, ranging from biology to chemistry and physics.[1b] They can be readily tuned across the visible and near infrared region of the spectrum by functionalizing them with electron donating and withdrawing groups.[2,3] Another approach to tune and enhance the chiroptical activity is based on the grafting of two achiral chromophores at the 2,15 extremities of carbo[6]helicene for instance. In this case and because the π-conjugation is limited through the whole helical backbone, the chromophores can interact through space, and give access to Exciton Coupling (EC) chirality.[3] In 2018, we investigated this phenomenon and have shown that this strategy can lead to intense and tuneable chiroptical properties, both in the ground- (electronic circular dichroism (ECD))[3a] and excited-state (circularly polarized luminescence (CPL) emission).[3b-d] Recently, Santoro, Schuster, Nuckolls et al. have observed strong amplification of the circular dichroic response in helicene-perylene-diimide (PDI) nanoribbons arising from an exciton-like coupling between two helicene units.[4] It is indeed well-known that when two or more identical chromophores are connected to close vicinal functions such as diols, diamines or other within a chiral molecule, they interact with each other and give rise to EC. Such phenomenon gives a remarkable pattern in ECD, consisting of bisignate Cotton effects, from the sign of which the absolute configuration of the molecule can be deduced, as depicted in Figure S1.1. Berova, Harada and Nakanishi[&] have developed this nonempirical approach called 'CD Exciton Chirality Method' and exhaustively used it to determine absolute configurations of many classes of chiral compounds and natural products.[5] Typically, the achiral chromophores used exhibit a strong electric dipole moment in preferred directions and their interaction gives rise to strong EC thanks to proximity through the chiral space. Porphyrins are archetypes of such chromophores[6] since they display highly intense absorption bands, especially the Soret one (epsilon ~ 420 000 M^{-1} cm^{-1} at 420 nm), planar geometry and ability to coordinate metallic ions such as Zn(II) and Mg(II).[7] Herein, we describe helicene-porphyrin conjugates to explore and rationalize the role of the helical π-conjugation in the EC phenomenon. We show that grafting two ethynyl-porphyrin units on the 2,15 positions of a carbo[6]helicene results in a clear and strong EC signature on the Soret band. While in previous examples of EC mediated by carbo[6]helicene,[3] the typical bisignate signature of the EC chirality was often hidden by additional strong helicenic-centered ECD bands, here the strong and localized Soret band leads to an almost isolated bisignate ECD response at 440 nm, which definitely ascertains the existence of EC chirality in helicenic derivatives, thus making porphyrins appealing tools to further reveal chiroptical effects in helicenes chemistry. We thus highlight the synergetic effect of helicenes and porphyrins[2c] in obtaining enhanced chiroptical responses in an absorption region where they are usually weak.

Enantiopure hexahelicene derivatives *P*- and *M*-**H6Pr1** consisting of 2,15-bis-ethynyl-carbo[6]helicene decorated with two phenyl-ethynyl-Zn-porphyrins at each extremity were prepared according to Figure 1a, *i.e.* through a Sonogashira coupling of either *P* or *M*-2,15-bis(4-ethynyl-phenyl-ethynyl)-carbo[6]helicene **H6PhH** with bromo-porphyrin **PrBr** in 19% yield under classical conditions. In the course of the reaction, a homocoupling of the mono-helicene-porphyrin intermediates also occurred through a Glaser-type coupling, giving also access to enantiopure compounds (*P*,*P*) and (*M*,*M*)-**H6Pr2** as side products in 16% yield. The metal-free porphyrin analogue **H6Pr3** was also prepared in quantitative yield by treating

[a] Univ Rennes, CNRS, ISCR - UMR 6226, F-35000 Rennes, France. ludovic.favereau@univ-rennes1.fr, jeanne.crassous@univ-rennes1.fr
[b] Department of Chemistry, University at Buffalo, State University of New York, Buffalo, USA. jochena@buffalo.edu
[c] Aix Marseille University, CNRS Centrale Marseille, iSm2, 13284 Marseille, France.
Electronic Supplementary Information (ESI) available: [details of any supplementary information available should be included here]. See DOI: 10.1039/x0xx00000x

H6Pr1 with trifluoroacetic acid. Compounds **H6Pr1**, **H6Pr2** and **H6Pr3** were fully characterized by ^{1}H and ^{13}C NMR spectroscopy and mass spectrometry (all details are provided in the Electronic Supporting Information, ESI). The **H6Pr1** and **H6Pr3** molecules show limited sets of resonances on their ^{1}H NMR spectra, thus revealing the highly symmetrical nature of the obtained chiral porphyrin molecules. The spectra depict the typical signatures of both the helicene and porphyrin units. For example, the C_2-symmetric **H6Pr1** displays only one set of signal typical of the fingerprint of symmetrically bis-substituted 2,15-ethynyl-carbo[6]helicene.[3] Furthermore, the β-pyrrolic protons that resonate between 9 and 9.85 ppm and the deshielded proton at 10.15 ppm corresponding to the free *meso* position in the porphyrin core were identified and assigned via 2D NMR experiments (see ESI). The signal of the inner pyrrolic NH protons in **H6Pr3** resonates at -2.39 ppm.[8]

The UV-vis absorption and ECD spectra of **H6Pr1**, **H6Pr2** and **H6Pr3** are depicted in Figures 1b and 1c, respectively. In the high energy region, *i.e.* below 460 nm, similar signatures are observed for these three compounds, with absorption bands at 298 (ε 68800 M^{-1} cm^{-1}), 345 (49700), and 361 (43000) nm assigned to π–π* transitions of the helicene unit, accompanied by the typically huge absorption signal at 440 nm (ε 480000 M^{-1} cm^{-1}), corresponding to the Soret band of the two porphyrin units. In the low energy part of the spectrum the typical porphyrin Q bands are observed, affording expectedly two distinct signals at 558 and 604 nm for the Zn-porphyrins (**H6Pr1** and **H6Pr3**) and four ones (525, 575, 662 and 688 nm) for the free-base chromophores (**HPr2**), all being of rather strong intensities (ε 30600 - 40000 M^{-1} cm^{-1}).

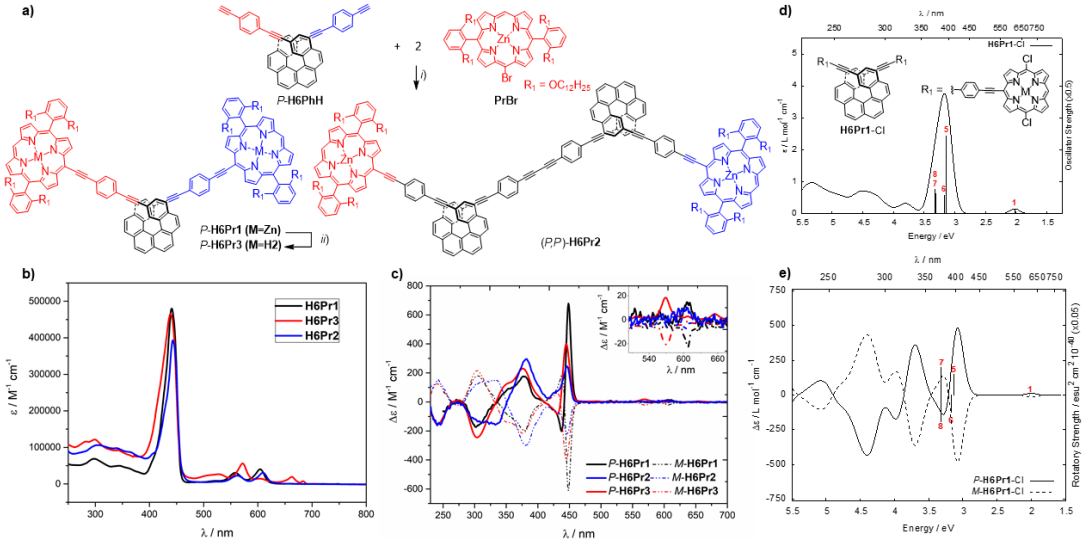

Figure 1. a) Synthetic pathway to **H6Pr1**, **H6Pr2** and **H6Pr3**. *i*) $Pd(PPh_3)_4$, CuI, Toluene/Et_3N; *ii*) TFA, DCM, TLC monitoring. Experimental b) UV-vis and c) ECD spectra of helicene-porphyrin conjugates **H6Pr1**, **H6Pr2** and **H6Pr3**, d) chemical structure of the calculated model **H6Pr1**-Cl and calculated UV-vis spectrum e) calculated mirror-image ECD spectra.

TD-DFT calculations with Gaussian 16 program,[9] LC-PBE0 functional,[10] def2-SV(P) basis[11] and the solvent (CH_2Cl_2) polarizable continuum model (PCM)[12] were performed on a truncated system of **H6Pr1**, where the $Ph(OR)_2$ substituents at the Zn-porphyrin units were replaced by chlorine atoms, denoted here as **H6Pr1**-Cl (see Figure 1d and ESI for further details and References 13a-b for overviews of the general performance of TD-DFT for chiroptical spectra). Different conformers of **H6Pr1**-Cl were considered, as shown in Figure S2.1. One of them is clearly dominant, with a Boltzmann population of 67% at 298 K, and was used for subsequent calculations accordingly. The calculated broadened absorption spectrum of **H6Pr1**-Cl agrees very well with the experimental spectrum for **H6Pr1**. The peaks are systematically blue shifted by 0.3 eV in the calculations (see Scheme S2.1), which is not uncommon. The weak lowest-energy/longest wavelength band in the **H6Pr1** spectrum is caused by an effectively degenerate pair of transitions, #1 and #2, which correspond to an exciton-coupled set of porphyrin Q band transitions (Figure S2.3 and Table S2.2). The contributing MOs are composed of in-phase and out-of-phase π and π* porphyrin fragment frontier orbitals (FFOs). The small energetic splitting indicates that the FFOs are only weakly coupled. The frontier MOs (FMOs) in **H6Pr1**-Cl are mostly localized on the porphyrins, but several of the MOs also extended over the π-conjugated systems of the phenyl (Ph) ring and the alkynyl (CC) groups, and reach into the helicene (Figure 2a). These MOs are therefore clearly perturbed, relative to isolated Zn-porphyrin. The second set of excitations, #3 and #4, around 2.1 eV, is assigned to coupling of the remaining Q-band porphyrin transitions. The Soret band has 4 underlying transitions in the calculation, and formally arise from the coupling of the two π → π* B-band excitations in each porphyrin. Excitation #5, at 395 nm, has by far the largest oscillator strength (4.882), and the leading contributions involve MOs that are mostly, but not entirely, porphyrin-centered. Excitations #6 and #8, under the same band, have important contributions from the HOMO-2, which is a helicene π-orbital. The excitations therefore have mixed character of helicene-to-porphyrin charge transfer (CT) and porphyrin π → π*. Bands below 350 nm are of strongly mixed character, varying porphyrin–linker–helicene contributions.

Interestingly, each of these bands is active in ECD spectroscopy, with the *P*-**H6Pr1** enantiomer displaying the typical negative ($\Delta\varepsilon$ -172 M^{-1} cm^{-1} at 302 nm) and positive bands (+89 and +175 M^{-1} cm^{-1} at 352 and 378 nm, respectively) of the helicenic part, and a bisignate feature (-200 at 438 and + 671 M^{-1} cm^{-1} at 449 nm) corresponding to EC coupling chirality of the Soret band. It is worth to note that the Q band at 605 nm is also CD-active ($\Delta\varepsilon$ +14 M^{-1} cm^{-1}). For **H6Pr3,** the absorption spectrum shows a similarity in the lowest-wavelength region (ca. 280-370 nm) assigned to helicene-centered π-to-π* transitions and bands located at 440 nm and 520-680 nm were assigned to the Soret and Q-bands, respectively. *P*-**H6Pr3** displays a slightly more intense but otherwise similar ECD below 430 nm as *P*-**H6Pr1**, such as a negative band at 304 nm ($\Delta\varepsilon$ -245 M^{-1} cm^{-1}) followed by positive ones (+120 and +230 M^{-1} cm^{-1} at 352 and 378 nm, respectively). The excitonic coupling signature was found also for the free porphyrin *P* enantiomer with a positive Cotton effect in the porphyrin Soret band ($\Delta\varepsilon$ -82 and +393 M^{-1} cm^{-1} at 430 nm and 446 nm, respectively) and the Q bands at 570 nm and 654 nm appeared also ECD active ($\Delta\varepsilon$ +18 M^{-1} cm^{-1}, 6 M^{-1} cm^{-1}, respectively).

The calculated ECD spectrum[13] of **H6Pr1**-Cl is in very good agreement with experiments (Scheme S2.2) and the assignment of the ECD bands are in line with the absorption peaks. Note that the distance between the two Zn^{2+} ions is evaluated to be around 2.83 nm, a length consistent with good interactions between the electric transition dipole moments. The question of interest is therefore: How much of the intensity of the peak-trough pattern seen in the experimental ECD spectrum of *P*-**H6Pr1** around 450 nm is a result of exciton coupling of the Zn-porphyrin B-band transitions? To this end, calculations were performed on different dimers in the same arrangement as in the model for *P*-**H6Pr1**, with increasingly large fragments in the center of the molecule removed, and dangling bonds capped with hydrogen (Figures 2b and S2.6). The gradual increase of the chromophore extension in the series of models leads to the lowering of energy of the excitations of porphyrin B-band parentage, such that in the largest dimer, (**Pr1-alkynyl-Ph-alkynyl**)$_2$, the intense positive/negative pair of ECD bands is almost aligned with those of *P*-**H6Pr1**-Cl. However, the presence of the helicene evidently plays a crucial role, as the intensity of the exciton CD couplet is much larger in the full system, and it is not nearly as conservative as those of the models. For further analysis, we also set up a dipole coupling model for the exciton ECD (Figure 2c), based on the excitations of a truncated version of *P*-**H6Pr1**-Cl (labeled as mono- **H6Pr1**-Cl) in which the [6]helicene is fully intact, but one of the Zn-porphyrins is removed (Figure S2.9). A visual comparison of the simulated ECD spectrum for mono-**H6Pr1**-Cl reflects similar features as the corresponding experimental spectrum of **H6Pr2** and the calculated ECD band at 390 nm is much weaker than for **H6Pr1**-Cl (Figure 2d and S2.16). Indeed, (*P*,*P*) and (*M*,*M*)-**H6Pr2** exhibit absorption bands at 302 (ε 105580 M^{-1} cm^{-1}), 347 (95350), 360 (88300), 441 (385290), 558 (23400), and 605 (31200) nm. The obtention of (*P*,*P*) and (*M*,*M*)-**H6Pr2** consisting of two porphyrin-ethynyl-phenyl-ethynyl-hexahelicenyl units connected by two phenyl-ethynyl bridges show absence of EC chirality in (*P*) and (*M*)-**H6Pr2** since in this case the Soret band displays only one CD-active signal at 446 nm ($\Delta\varepsilon$ +228 M^{-1} cm^{-1}) and no apparent significant Exciton Coupling due to the very long distance between the two porphyrin cores. Other ECD active bands are found at 334 (-150) and 380 (+289) nm and correspond to the helicenic parts. Note that the negative band originating from the helicene units is strongly red-shifted compared to **H6Pr1** and the **H6PhH** precursor most probably as a result of strongly extended π-conjugation of the molecule. These results nicely illustrate how molecular engineering using either extended π-conjugation (**H6Pr2**) or functionalization with strongly polarizable units in close proximity (**H6Pr1** and **H6Pr3**) enables fine tuning of the chiroptical signatures. Satisfyingly, we have found that these derivatives display efficient fluorescence spectra (between 600 and 800 nm), with quantum yields between 16-25 % and moderate circularly polarized emission with dissymmetry factors g_{lum} around ±7. 10^{-4} ± for **H6Pr1** and **H6Pr2**, respectively, and around ±2.10^{-4} for **H6Pr3** (positive for the *P* enantiomer and vice versa, see Figures S1.27 and S1.28).[2,16,17]

Conclusions

Introducing porphyrin substituents into helicenic scaffolds in their 2,15 positions unambiguously confirms the presence and effectiveness of EC chirality in helicenes through the very strong bisignate ECD response in the Soret band (together with slightly ECD-active Q-bands). Compared to more classical examples displaying EC chirality, in which case achiral π-chromophores are generally linked to the chiral system through ester links, here the alkynyl groups are part of the two achiral π-chromophores. The latter interact predominantly through space, because the π-conjugation through the helix is partly broken. In addition, the helicene unit leads to a higher intensity of the EC response in comparison to fully non-conjugately assembled dyes. This specific finding may have several implications in the near future: these helical porphyrin systems may be used as chiral materials for photovoltaic devices,[14] they may show interesting phenomena involving spin selectivity[15] or may be used for detection of chiral substrates.[5] Finally, this strategy enables access to CPL active porphyrin derivatives which still remains quite rare,[16,17] and thus opens new opportunities for the design of efficient far-red and near-infrared CPL emitters.

Conflicts of interest

There are no conflicts to declare.

Acknowledgments

We thank the Centre National de la Recherche Scientifique (CNRS) and the University of Rennes. P.M. thanks the European Commission Research Executive Agency (Grant

Agreement number: 859752 — HEL4CHIROLED — H2020-MSCA-ITN-2019) for financial support. J.A. acknowledges the Center for Computational Research (CCR, University at Buffalo, http://hdl.handle.net/10477/79221) and grant CHE-1855470 from the National Science Foundation for support of the theoretical component of this study. JASCO Europe is warmly thanked for their assistance in measuring CPL of **H6Pr1** enantiomers.

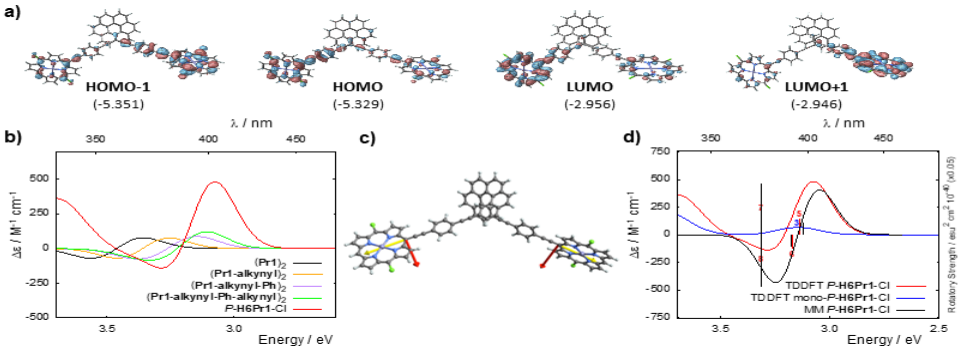

Figure 2. a) Isosurfaces (0.020 au) of the frontier molecular orbitals (FMOs) involved in the selected transitions for *P*-**H6Pr1**-Cl. Values listed in parentheses are the corresponding orbital energies in eV. b) Comparison of the low energy region of the ECD spectrum for *P*-**H6Pr1**-Cl and the corresponding dimer models of Figure S2.5. c) Set-up of electric transition dipole moment (TDM) vectors based on excitations #3 (yellow) and #4 (red) of mono-*P*-**H6Pr1**-Cl for exciton coupling 'matrix method' model for *P*-**H6Pr1**-Cl, and the rotated set of TDMs, shown together with the full structure of *P*-**H6Pr1**-Cl. d) Low-energy regions of the ECD spectra of the mono-*P*-**H6Pr1**-Cl and *P*-**H6Pr1**-Cl from TDDFT calculations and from the matrix method (MM) dipole-coupling model. MM dipole-coupling model based on excitations #3 and #4 of mono-*P*-**H6Pr1**-Cl. Selected transitions and rotatory strengths are indicated as 'stick spectra'.

Notes and references

1 a) C.-F. Chen, Y. Shen, 'Helicene Chemistry: From Synthesis to Applications'; Springer Berlin Heidelberg: Berlin, Heidelberg, 2017; b) M. Gingras, *Chem. Soc. Rev.* 2013, **42**, 1051-1095; c) K. Dhbaibi, L. Favereau, J. Crassous, *Chem. Rev.* 2019, **119**, 8846-8953.

2 Selected examples: a) J. Bosson, G. M. Labrador, C. Besnard, D. Jacquemin, J. Lacour, *Angew. Chem. Int. Ed.* 2021, **133**, 8815-8820; b) R. Duwald, J. Bosson, S. Pascal, S. Grass, F. Zinna, C. Besnard, L. Di Bari, D. Jacquemin, J. Lacour, *Chem. Sci.* 2020, **11**, 1165-1169; c) K. Kato, K. Furukawa, T. Mori, A. Osuka, *Chem. Eur. J.* 2018, **24**, 572-575.

3 a) R. Bouvier, R. Durand, L. Favereau, M. Srebro-Hooper, V. Dorcet, T. Roisnel, N. Vanthuyne, Y. Vesga, J. Donnelly, F. Hernandez, J. Autschbach, Y. Trolez, J. Crassous, *Chem. Eur. J.* 2018, **24**, 14484-14494 ; b) K. Dhbaibi, L. Favereau, M. Srebro-Hooper, M. Jean, N. Vanthuyne, F. Zinna, B. Jamoussi, L. Di Bari, J. Autschbach, J. Crassous, *Chem. Sci.* 2018, **9**, 735-742; c) K. Dhbaibi, L. Favereau, M. Srebro-Hooper, C. Quinton, N. Vanthuyne, L. Arrico, T. Roisnel, B. Jamoussi, C. Poriel, C. Cabanetos, J. Autschbach, J. Crassous, *Chem. Sci.* 2020, **11**, 567-576; d) K. Dhbaibi, C. Shen, M. Jean, N. Vanthuyne, T. Roisnel, M. Górecki, B. Jamoussi, L. Favereau, J. Crassous, *Front. Chem.* 2020, **8**, 237 ; e) C. Shen, F. Gan, G. Zhang, Y. Ding, J. Wang, R. Wang, J. Crassous, H. Qiu, *Mater. Chem. Front.*, 2020, **4**, 837-844; f) K. Dhbaibi, L. Abella, S. Meunier-Della-Gatta, T. Roisnel, N. Vanthuyne, B. Jamoussi, G. Pieters, B. Racine, E. Quesnel, J. Autschbach, J. Crassous, L. Favereau, *Chem. Sci.* 2021, **12**, 5522-5533.

4 a) X. Xiao, S. K. Pedersen, D. Aranda, J. Yang, R. A. Wiscons, M. Pittelkow, M. L. Steigerwald, F. Santoro, N. J. Schuster, C. Nuckolls *J. Am. Chem. Soc.* 2021, **143**, 983-991; b) D. Aranda, N. J. Schuster, X. Xiao, F. J. Ávila Ferrer, F. Santoro, Colin Nuckolls, *J. Phys. Chem. C* 2021, **125**, 2554-2564.

5 a) N. Harada, K. Nakanishi, N. Berova, in *Comprehensive Chiroptical* Spectroscopy, John Wiley & Sons, Inc., 2012, p. 115; b) N. Berova, L. D. Bari, G. Pescitelli, *Chem. Soc. Rev.* 2007, **36**, 914; c) X. Huang, K. Nakanishi, N. Berova, N. *Chirality* 2000, **12**, 237-255.

6 G. Pescitelli, S. Gabriel, Y. Wang, J. Fleischhauer, R. W. Woody, N. Berova, *J. Am. Chem. Soc.* 2003, **125**, 7613-7628.

7 a) Dolphin, D. The Porphyrins; Academic Press: New York, 1979; b) The Porphyrin Handbook; Kadish, K. M., Smith, K. M., Guilard, R., Eds.; Academic Press: San Diego, 2000; Vol. 1–20 ; c) For a review on optically active porphyrins, see: c) H. Lu, N. Kobayashi, *Chem. Rev.* 2016, **116**, 6184-6261. For a seminal review on the spectra of porphyrins, see: d) M. Gouterman, *J. Mol. Spec.* 1961, **6**, 138-163.

8 S. Hiroto, Y. Miyake, H. Shinokubo, *Chem. Rev.* 2017, **117**, 2910–3043.

9 M. J. Frisch, G. W. Trucks, H. B. Schlegel et al. "Gaussian 16, Revision B.01", Gaussian, Inc., Wallingford CT, 2016. URL: www.gaussian.com.

10 A) C. Adamo, V. Barone, *J. Chem. Phys.*, 1999, **110**, 6158-69; b) T. Yanai, D. P. Tew, N. C. Handy, *Chem. Phys. Lett*. 2004, **393**, 51; c) J. Autschbach, M. Srebro, *Acc. Chem. Res.* 2014, **47**, 2592.

11 a) F. Weigend, R. Ahlrichs, *Phys. Chem. Chem. Phys.* 2005, **7**, 3297-305; b) F. Weigend, *Phys. Chem. Chem. Phys.* 2006, **8**, 1057-65.

12 G. Scalmani, M. J. Frisch, *J. Chem. Phys.*, **2010**, 132, 114110.

13 a) M. Srebro-Hooper, J. Autschbach, *Annu. Rev. Phys. Chem.* 2017, **68**, 399-420; b) J. Autschbach, L. Nitsch-Velasquez, M. Rudolph, *Top. Curr. Chem.* 2011, **298**, 1-98.

14 a) K. Ladomenou, T. Kitsopoulos., G. Sharma, and A. Coutsolelos, *RSC Adv*. 2014, **4**, 21379-21404; b) J. M. Pa , J. H. Lee, W.-D. Jang, *Coord. Chem. Rev.* 2020, **407**, 213157; c) Y.-J. Chiang, Y.-H. Hsiao, Y.-H. Chen, C.-M. Hung, H.-C. Chen, C.-Y. Yeh, *ACS Energy Lett.* 2020 **5**, 2641-2650; d) S. Mathew, A. Yella, P. Gao, R. Humphry-Baker, B. F. Curchod, N. Ashari-Astani, I. Tavernelli, U. Rothlisberger, M. K. Nazeeruddin, M. Grätzel, *Nat. Chem.* 2014, **6**, 242-247; e) K. Zeng, Z. Tong, L. Ma, W. -H. Zhu, W. Wu,Y. Xie, *Energy Environ. Sci*. 2020, **13**, 1617-1657.

15 a) R. Naaman, Y. Paltiel, D. H. Waldeck, *Nature Rev. Chem*. 2019, **3**, 250-260; b) G. Bullard, F. Tassinari, C.-H. Ko, A. K. Mondal, R. Wang, S. Mishra, R. Naaman, M. J. Therien, *J. Am. Chem. Soc*. 2019, **141**, 14707-14711.

16 C. Maeda, K. Ogawa, K. Sadanaga, K. Takaishi, T. Ema, *Chem. Commun.* 2019, **55**, 1064-1067.

17 a) W.-L. Zhao, M. Li, H.-Y. Lu, C.-F. Chen, *Chem. Commun.* 2019, **55**, 13793-13803; b) J. Crassous in "Circularly Polarized Luminescence of Isolated Small Organic Molecules", T. Mori (ed.), Springer, 2020, chap. 4, pp 53-97.